Plane Wave Synthesis in a Reconfigurable Over-the-air Chamber

Matthew D. Arnold†, Rashid Mehmood†, Jon W. Wallace*, and Michael A. Jensen†

†Brigham Young University, Provo, UT, USA
E-mail: r.mehmood@ieee.org, jensen@byu.edu

*Lafayette College, Easton, PA, USA
E-mail: wall@ieee.org

***Abstract*—This work explores the accuracy with which a reconfigurable over-the-air chamber is able to synthesize a plane wave, as a basic component of a multipath field, in a test zone in which a wireless device under test is to be placed for performance evaluation. The excitations and reflection coefficients required to synthesize the plane wave are determined from a gradient descent optimization seeded with a convex optimization of a linear approximation of the problem. Results show that the chamber is able to synthesize a plane wave with high fidelity over a test zone circle whose diameter is approximately 40% of the chamber side dimension.**

I. Introduction

Over-the-air (OTA) testing of wireless devices has become increasingly important as multi-antenna techniques have gained traction in mobile communications. While most OTA systems use either a multi-probe anechoic chamber [1] or a mode-stirred reverberation chamber [2], we have demonstrated a reconfigurable OTA chamber (ROTAC) that enables increased flexibility in synthesizing multipath fields in a reverberation chamber without the high cost and complexity of an anechoic arrangement [3], [4]. While our prior work has shown the potential of this concept, more work is required to fully assess the capabilities of the technology. The objective of this work is to determine the accuracy with which the ROTAC can generate a single plane wave in the test or *quiet zone* in the chamber, recognizing that the plane wave forms a fundamental component for any synthesized multipath environment.

II. Analysis

The ROTAC used is a cubical resonant metallic cavity with a side length of 30 cm as shown in Figure 1. Each cube face except the bottom is lined with a 3×3 grid of equally spaced monopole antennas, resulting in $N_{\mathrm{P}} = 45$ antenna ports. Finite-difference time-domain simulations are used to compute the electric field inside the chamber for a given port excitation and matched antenna terminations as well as the system S-parameter matrix [3]. A small number N_{F} of ROTAC *feed* ports are used to excite the chamber, and the remaining N_{R} *RE* ports are terminated with reconfigurable impedance elements (REs) to control the reflections of waves from the walls. The electric field at a kth location inside the chamber can be expressed as [3]

$$e_k = \left[\mathbf{e}_{\mathrm{F},k}^{\mathrm{T}} + \mathbf{e}_{\mathrm{R},k}^{\mathrm{T}} \boldsymbol{\Gamma}(\mathbf{I} - \mathbf{S}_{\mathrm{RR}}\boldsymbol{\Gamma})^{-1}\mathbf{S}_{\mathrm{RF}}\right] \mathbf{a}_{\mathrm{F}}, \tag{1}$$

where $\mathbf{e}_{\mathrm{F},k}$ and $\mathbf{e}_{\mathrm{R},k}$ are $N_{\mathrm{F}} \times 1$ and $N_{\mathrm{R}} \times 1$ vectors containing the electric field at the kth location based on a unit excitation of feed and RE ports, respectively, $\{\cdot\}^{\mathrm{T}}$ is the transpose, $\boldsymbol{\Gamma}$ is the $N_{\mathrm{R}} \times N_{\mathrm{R}}$ diagonal matrix representing the reflection coefficients on the RE ports, $\mathbf{S}_{\mathrm{RR}}$ and $\mathbf{S}_{\mathrm{RF}}$ are $N_{\mathrm{R}} \times N_{\mathrm{R}}$ and $N_{\mathrm{R}} \times N_{\mathrm{F}}$ S-parameter matrices for coupling between RE ports and between feed and RE ports, respectively, and $\mathbf{a}_{\mathrm{F}}$ is the $N_{\mathrm{F}} \times 1$ vector of feed port excitations. Each RE has a complex reflection coefficient $\Gamma_{ii} = \gamma_i$, where $|\gamma_i| \leq 1$.

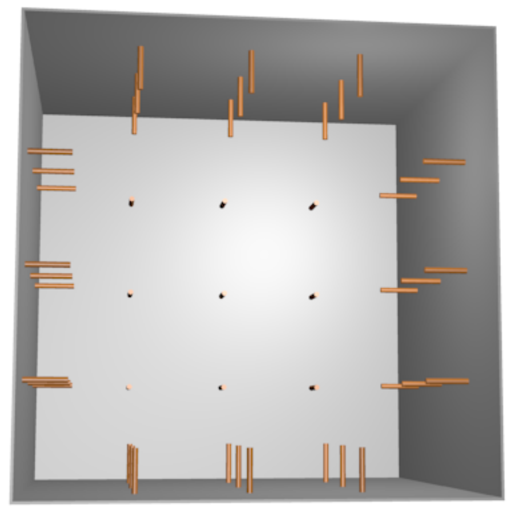

Fig. 1. ROTAC model, where the bottom panel has been removed to allow visualization of the chamber interior.

An idealized plane wave at the kth location (x_k, y_k) and propagating at the angle ϕ can be expressed as

$$e_{\mathrm{p},k}(\phi) = \alpha \exp[-jk_0(x_k \cos\phi + y_k \sin\phi)], \tag{2}$$

where α is the plane wave magnitude and k_0 is the free space wavenumber computed here at $f = 2.55$ GHz. Our goal is to find the value of $\boldsymbol{\gamma}$ – the vector of RE reflection coefficients – that minimizes the fitness function

$$f(\boldsymbol{\gamma}) = \|\mathcal{E}(\boldsymbol{\gamma})\|^2 = \|\mathbf{e}(\boldsymbol{\gamma}) - \mathbf{e}_{\mathrm{p}}(\phi)\|^2, \tag{3}$$

where $\|\cdot\|$ is the L2 norm and $\mathbf{e}(\boldsymbol{\gamma})$ and $\mathbf{e}_{\mathrm{p}}(\phi)$ are the column wise stacked versions of (1) and (2), respectively.

We optimize to find $\boldsymbol{\gamma}$ using gradient descent (GD) [4]. To initialize the GD iteration, we linearize (1) by taking the first term of the Neumann expansion of $(\mathbf{I} - \mathbf{S}_{\mathrm{RR}}\boldsymbol{\Gamma})^{-1}$, with the resulting vector denoted as $\hat{\mathbf{e}}(\boldsymbol{\gamma})$. We can then minimize $\|\hat{\mathbf{e}}(\boldsymbol{\gamma}) - \mathbf{e}_{\mathrm{p}}(\phi)\|$ subject to the constraint $\gamma_i \gamma_i^* \leq 1$, where $\{\cdot\}^*$ is the complex conjugate, using convex optimization [5].

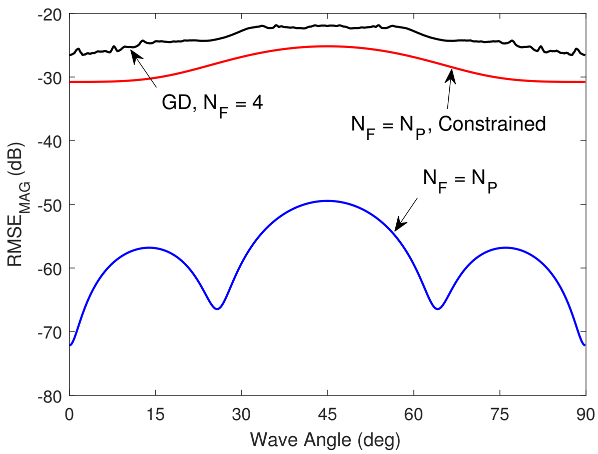

Fig. 2. Magnitude error versus desired plane wave angle for different ROTAC configurations.

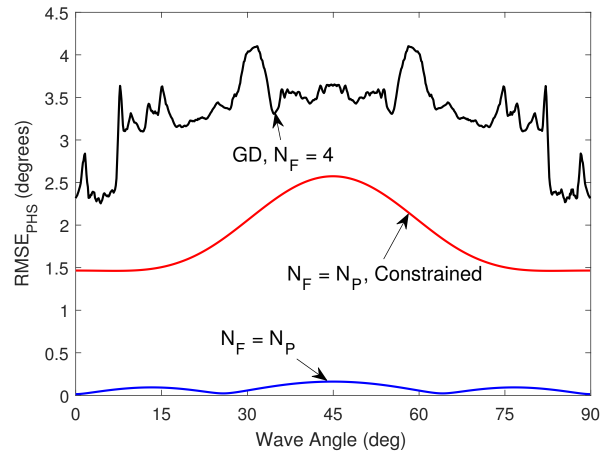

Fig. 3. Phase error versus desired plane wave angle for different ROTAC configurations.

The solution to this optimization yields the estimate $\boldsymbol{\gamma}_0$ that is refined using the GD iteration

$$\boldsymbol{\gamma}_{m+1} = \boldsymbol{\gamma}_m - \delta \nabla f(\boldsymbol{\gamma}), \tag{4}$$

where m is the iteration index, δ is the step size, and the gradient $\nabla f(\boldsymbol{\gamma})$ can be computed in closed form.

It is interesting to compare the results of this optimization to the case when all ports are fed, or $N_{\mathrm{F}} = N_{\mathrm{P}}$. In this case, the field at the kth point is given by $\hat{e}_k = \mathbf{e}_{\mathrm{F},k}^{\mathrm{T}} \hat{\mathbf{a}}_{\mathrm{F}}$. The incident voltages $\hat{\mathbf{a}}_{\mathrm{F}}$ can be computed by setting $\hat{e}_k = e_{\mathrm{p},k}$ and applying the least squares solution $\hat{\mathbf{a}}_{\mathrm{F}} = \mathbf{D}^{+}\mathbf{e}_{\mathrm{p}}(\phi)$, where $(\cdot)^{+}$ is the Moore-Penrose pseudo-inverse and $\mathbf{D}$ is the matrix whose kth row is $\mathbf{e}_{\mathrm{F},k}^{\mathrm{T}}$. Since this solution does not constrain the input power to the chamber, we can also formulate the problem as a convex optimization that minimizes $\|\mathbf{D}\hat{\mathbf{a}}_{\mathrm{F}} - \mathbf{e}_{\mathrm{p}}(\phi)\|$ subject to $\|\hat{\mathbf{a}}_{\mathrm{F}}\| \leq \sqrt{\beta}$, where β refers to the total chamber input power.

III. Results

We assume a quiet zone circle of radius $r = 6$ cm at the chamber center and for the GD optimization choose the $N_{\mathrm{F}} = 4$ feed ports on the center of each chamber side. For both the GD and the power-constrained $N_{\mathrm{F}} = N_{\mathrm{P}}$ optimization, we choose α (plane wave magnitude) to minimize the root mean squared error (RMSE) between the synthesized and desired fields. Figures 2 and 3 plot the normalized RMSE of the field magnitude and phase, computed as

$$\mathrm{RMSE}_{\mathrm{MAG}} = \sqrt{\frac{\sum_{k=1}^{K} \left[|e_k(\boldsymbol{\gamma})| - |e_{\mathrm{p},k}(\phi)|\right]^2}{\sum_{k=1}^{K} |e_{\mathrm{p},k}(\phi)|^2}}, \tag{5}$$

$$\mathrm{RMSE}_{\mathrm{PHS}} = \sqrt{\frac{1}{K} \sum_{k=1}^{K} \left[\angle e_k(\boldsymbol{\gamma}) e_{\mathrm{p},k}^{*}(\phi)\right]^2}, \tag{6}$$

where K is the total number of field observation points, versus the plane wave angle ϕ for our three solutions. The results are computed at the interval $\Delta\phi = 1/8^{\circ}$ and smoothed with a 5-sample moving average window, after which the magnitude result is converted to dB ($20\log_{10}(\cdot)$). While $N_{\mathrm{F}} = N_{\mathrm{P}}$ results in the lowest error, when the total input power is constrained ($\beta = 4$), we observe that the RMSE increases considerably. As expected, the GD optimization with $N_{\mathrm{F}} = 4$ produces the largest error, although its performance is not significantly worse than that achieved for $N_{\mathrm{F}} = N_{\mathrm{P}}$ under the power constraint, with a peak magnitude error of under 20 dB and a peak phase error of 4.2°. Magnitude and phase error can be reduced by either increasing the size of the chamber or by reducing the size of the quiet zone. Overall the results are encouraging and indicate that plane wave synthesis is feasible with a relatively compact ROTAC.

IV. Conclusion

This work evaluates the ability of a ROTAC to synthesize a plane wave over a specified quiet zone. Simulation results for a circular quiet zone of radius 6 cm in a cubical chamber of side length 30 cm demonstrate that the ROTAC can effectively synthesize a plane wave with relatively low magnitude and phase error. This work will be augmented in the future by studying the behavior for different chamber sizes, numbers of ports, and quiet zone sizes.

References

[1] P. Kyösti, J. P. Nuutinen, and T. Jämsä, "MIMO OTA test concept with experimental and simulated verification," in *Proc. 4th European Conf. on Antennas and Propagation*, Barcelona, Spain, Apr. 2010.

[2] M. A. Garcia-Fernandez, J. D. Sanchez-Heredia, A. M. Martinez-Gonzalez, D. A. Sanchez-Hernandez, and J. F. Valenzuela-Valdes, "Advances in mode-stirred reverberation chambers for wireless communication performance evaluation," *IEEE Commun. Mag.*, vol. 49, no. 7, pp. 140–147, July 2011.

[3] R. Mehmood, J. W. Wallace, and M. A. Jensen, "Reconfigurable OTA chamber for MIMO wireless device testing," in *Proc. 10th European Conf. on Antennas and Propagation*, Davos, Switzerland, Apr. 2016.

[4] Matthew D Arnold, Rashid Mahmood, Jon W Wallace, and Michael A Jensen, "Efficient optimization method for a reconfigurable OTA chamber," in *Proc. IEEE Intl. Symp. on Antennas and Propagation*, San Diego, California, 2017, IEEE, pp. 1421–1422.

[5] CVX Research Inc., "CVX: Matlab software for disciplined convex programming, version 2.0.," April 2011.